LCD Motion Blur: Modeling, Analysis, and Algorithm

Article *in* IEEE Transactions on Image Processing · August 2011

DOI: 10.1109/TIP.2011.2109728 · Source: PubMed

Stanley H. Chan
Harvard University
33 PUBLICATIONS **1,157** CITATIONS
SEE PROFILE

Truong Q. Nguyen
University of California, San Diego
198 PUBLICATIONS **4,328** CITATIONS
SEE PROFILE

LCD Motion Blur: Modeling, Analysis and Algorithm

Stanley H. Chan, *Student Member, IEEE,* and Truong Q. Nguyen, *Fellow, IEEE.*

***Abstract*—Liquid crystal display (LCD) devices are well known for their slow responses due to the physical limitations of liquid crystals. Therefore, fast moving objects in a scene are often perceived as blurred. This effect is known as the LCD motion blur. In order to reduce LCD motion blur, an accurate LCD model and an efficient deblurring algorithm are needed. However, existing LCD motion blur models are insufficient to reflect the limitation of human eye tracking system. Also, the spatio-temporal equivalence in LCD motion blur models has not been proven directly in the discrete two-dimensional spatial domain, although it is widely used.**

There are three main contributions of this paper: modeling, analysis and algorithm. First, a comprehensive LCD motion blur model is presented, in which human eye tracking limits are taken into consideration. Second, a complete analysis of spatio-temporal equivalence are provided and verified using real video sequences. Third, an LCD motion blur reduction algorithm is proposed. The proposed algorithm solves an l_1-norm regularized least-squares minimization problem using a subgradient projection method. Numerical results show that the proposed algorithm gives higher PSNR, lower temporal error and lower spatial error than motion compensated inverse filtering (MCIF) and Lucy-Richardson deconvolution algorithm, which are two state-of-the-art LCD deblurring algorithms.

***Index Terms*—Liquid crystal displays, LCD, motion blur, human visual system, subgradient projection, spatial consistency, temporal consistency**

I. Introduction

LIQUID Crystal Display (LCD) devices are known to have slow responses due to the physical limitations of liquid crystals (LC). LC are organic fluids that exhibit both liquid and crystalline like properties. They do not emit light by themselves, but the polarization phase can be changed by electric fields [1]. A common circuit used in LCD to control the electric fields is known as the thin film transistor (TFT) [2]. Although TFT responds quickly, it takes some time for the LC to change its phase. This latency is known as the fall time if the signal is changing from high to low or the rise time if the signal is changing from low to high. Since the fall and rise time are not infinitesimal, the step response of an LC exhibits a sample-hold characteristic (see Fig. 1).

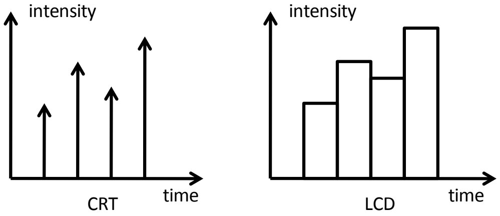

Fig. 1. The signaling characteristics of a cathode ray tube (CRT) and a liquid crystal display (LCD). CRT shows spontaneous response, whereas LCD demonstrates a sample-hold response.

Compared to LCD, traditional cathode ray tube (CRT) displays do not have the sample-hold characteristic. When a phosphor is exposed to electrons, it starts to emit light. As soon as the electrons leave, the phosphor stops emitting light. The latency of a phosphor is typically between 20μs to 50μs [2], but the time interval between two frames is 16.67ms for a 60 frame per second video sequence. In other words, the latency of a phosphor becomes negligible compared to the frame interval.

Due to the sample-hold characteristic of liquid crystals, fast moving scenes displayed on the LCD are often seen blurred. This phenomenon is known as the LCD *motion* blur. We emphasize the word "motion" because if the scene is stationary, LCD and CRT will give essentially the same degree of sharpness.

A. Review of existing methods

There are a number of methods to reduce LCD motion blur. Back light flashing presented by Fisekovi et al [3] is one of the earliest methods. In this method, the back light (typically a cold cathode fluorescent lamp, CCFL) is controlled by a pulse-width modulation (PWM) [4]. Back light flashing reduces motion blur but it also causes fluctuation in luminance. If the flashing rate is not high enough, the luminance fluctuation can be seen by human eyes, hence causing eye strains. Therefore, in order to surpass the human eye limit (MPRT [1] 5.7ms, [6]), some advanced CCFL control methods are used, such as the active lamp technique presented by Yoon et al [6].

Signal over-drive [7] is another commonly used method to reduce motion blur. The motivation to over-drive a signal is that the phase change of an LC is faster if the electric field is stronger. This phenomenon is explained in [1] and experimentally verified in [8]. Therefore, if the input signal is changing from 0 to 200 (in gray scale), then instead of sending a signal from 0 to 200, the over-drive circuit produces a signal from 0 to 210 (or a different value, depending on the

Manuscript received XXX.

S. Chan and T. Nguyen are with the Department of Electrical and Computer Engineering, University of California, San Diego. Website: http://videoprocessing.ucsd.edu/∼stanleychan. Contact email: S. Chan: h5chan@ucsd.edu, T. Nguyen: nguyent@ece.ucsd.edu.

[1] MPRT stands for motion picture response time. [5]

circuit). Signal over-driving is often implemented using a look-up table, and a particular value is determined by the intensity change of a pixel. Image contents such as spatial and temporal consistencies are not considered.

Frame rate up conversion (FRUC) schemes is the third class of methods. The motivation of FRUC is that if the LC response can be improved, then the frame rate of LCD should also be increased. There are two major FRUC methods in the market: one is black frame insertion as presented by Hong et al [9], and the other one is full frame insertion presented in many papers such as [10], [11], [12], [13], [14]. Fig. 2 illustrates these two FRUC methods.

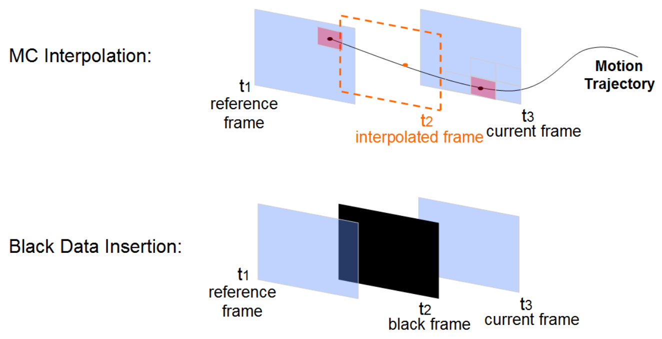

Fig. 2. Two commonly used frame rate up conversion method (FRUC). Top: full frame insertion method by motion compensation (MC). Bottom: black frame insertion method.

The last class of methods is the signal processing approach in which the input signal is over-sharpened so that it can compensate the motion blur caused by the LCD. Among all the methods, the motion compensated inverse filtering (MCIF) techniques presented by Klompenhouwer and Velthoven [15] is the most popular one. MCIF first models motion blur as a finite impulse response (FIR) filter. Then it finds an approximated inverse of the FIR filter to over-sharpen the image. MCIF can also be used together with frame rate up conversion scheme, as presented in [16]. Another signal processing approach is the deconvolution method proposed by Har-Noy and Nguyen [17]. In [17], the authors show that the deconvolution method gives better image quality than MCIF in terms of peak signal to noise ratio (PSNR) and visual subjective tests.

B. Objectives and Related Work

There are three objectives of this paper: modeling, simulation and algorithm.

First of all, we present a mathematical model for the hold-type LCD motion blur in the spatio-temporal domain. We do not consider the problem in the frequency domain as Klompenhouwer does in [15], because a video sequence is intrinsically a space-time signal [18]. It is more intuitive to study the motion blur in the spatio-temporal domain directly.

The modeling part of this paper is a generalization of [19]. In [19], Pan, Feng and Daly show a fundamental equation for LCD motion blur modeling (Equation (7) of [19]). However, they implicitly assume that the human eyes are able to track objects perfectly. This is not true in general because our eyes have only limited range of tracking speed (See Section III). The same finding is reported by He et al [20]. However, He et al do not explain the cause of such a limit and they do not justify their MCIF design from a human visual system point of view. In contrast, our study of the eye tracking limit is based on literature of cognitive science, and verified using subjective tests.

The second objective of this paper is to provide a tool for the simulation of motion blur. A limitation of Pan's equation (Equation (7) of [19]) is that the integration has to be performed in the temporal domain. To do so, the time step of the integration should be small, for otherwise the integration cannot be approximated using a finite sum. Since the frame rate of a video sequence is fixed, in order to make the time step small, we need to interpolate intermediate frames. Temporal interpolation is time consuming: If the time step is 1/10 of the time interval between frames, then 10 intermediate frames are needed. Therefore, the simulation of motion blur will be difficult unless there is an alternative method, which will be discussed in Section II.

The spatio-temporal equivalence has been used extensively in the literature but not proved. For example, Kurita [21] used the spatio-temporal equivalence to improve LCD image quality; Becker used the spatio- temporal equivalence to show the relation between blur edge width (BEW) and blur edge time (BET) for back light scanning [4]; Tourancheau used the spatio- temporal equivalence to compare four commercially available LCD TVs [22]; Klompenhouwer showed the relation between BEW and frequency response of the blur operation (known as the temporal MTF) [23]. Yet, none of these papers attempted to prove the spatio-temporal equivalence rigorously.

The most relevant paper in proving the spatio-temporal equivalence is [24]. Klompenhouwer drew a connection between the spatial and temporal aperture in a somewhat different - and very elegant - manner. However, a precise numerical approximation scheme for evaluating the continuous time integration in the discrete spatial domain is not pursued. Also, Klompenhouwer's paper is focused on the unit step input signal (which is a one-dimensional signal), whereas our work focuses on the general video signals.

The third objective of this paper is to propose a deconvolution algorithm based on the spatio-temporal equivalence.

A limitation of Klompenhouwer and Velthoven's MCIF [15] is that the MCIF cannot take into account of the spatial and temporal consistencies. Spatial consistency means that a pixel should have a value similar to its neighbors, unless it is along an edge in an image. Temporal consistency means that a pixel value should not change abruptly along the time axis, for otherwise it will be seen as flickering artifacts. In this paper, we use a spatial regularization function to penalize variations in the spatial domain caused by noise. The l_1 normed regularization function used in our method is able to suppress the noise while preserving the edges. We also use a temporal regularization function to maintain the smoothness of the images along the time axis. In [25], Yao et al proposed similar regularization functions in the context of coding artifacts removal. However, their problem setup is easier than ours because there is no blurring operators in their problem.

C. Organization

The organization of this paper is as follows. In Section II we prove the spatio-temporal equivalence. We show by experiments that the spatial approximation to the temporal integration is accurate. In Section III we present the findings of human eye tracking limits. Visual subjective tests are used to determine the optimal length of the FIR motion blur filter. In Section IV we present the proposed algorithm. Comparisons with MCIF and Lucy-Richardson algorithm are discusses.

II. Spatio-Temporal Equivalence

A. Review of LCD motion blur model

For completeness, we provide a brief introduction to the LCD motion blur model. Most of the material presented in this subsection is due to Pan, Feng and Daly [19].

Let $I_c(x, y, t)$ be a frame sampled at time t and suppose $I_c(x, y, t)$ has a motion vector (v_x, v_y). Let $h_D(t)$ be the step response of the display, where the subscript D can either be CRT or LCD. By Pan, Feng and Daly [19], the image shown on the display is

$$I_s(x, y, t) = \int_{-\infty}^{\infty} h_D(\tau) I_c(x+v_x(t-\tau), y+v_y(t-\tau), t-\tau) d\tau. \tag{1}$$

An implicit assumption used in [19] is that the human eye tracking system is perfect, meaning that we can track any motion at any speed. Based on this, the motion compensated image formed on the retina becomes

$$\begin{aligned} I_m(x, y, t) &= I_s(x - v_x t, y - v_y t, t) \quad \text{[perfect eye tracking]} \\ &= \int_{-\infty}^{\infty} h_D(\tau) I_c(x - v_x\tau, y - v_y\tau, t - \tau) d\tau. \quad (2) \end{aligned}$$

Now assume that there is no low pass filtering of the HVS, then the observed signal becomes

$$I_o(x, y, y) = \int_{-\infty}^{\infty} h_D(\tau) I_c(x - v_x\tau, y - v_y\tau, t - \tau) d\tau. \tag{3}$$

To facilitate the discussion of this paper, we focus on the hold-type LCD. In this case, the step response of LCD is given by a boxcar signal, that is $h_{LCD}(t) = 1/T$ for $0 \le t \le T$ and $= 0$ for otherwise. With this setup, the image shown by an LCD is

$$I_o^{LCD}(x, y, t) = \frac{1}{T} \int_0^T I_c(x - v_x\tau, y - v_y\tau, t - \tau) d\tau. \tag{4}$$

B. Proof of Spatio-Temporal Equivalence

The integral in Equation (4) can be evaluated by performing an integration over time $0 \le t \le T$. However, for a digitized version of the signal $I_c(x, y, t)$, there is no information between two consecutive frames. Therefore, it is never possible to compute the integral exactly. To alleviate this issue, an approximation scheme must be used. In the followings, we discuss a spatio-temporal equivalence that allows us to approximate the temporal integration (4) by a spatial integration. But before we discuss the main theorem, we would like to provide some intuitive arguments.

Fig. 3 shows a video sequence. When integrating (4), we are essentially taking an average over the pixel values at a fixed position but at different time instants. Since all frames are highly correlated to each other (assume that there is no abrupt motions), we can approximate the average over different time instants as a spatial average over the pixel's neighborhoods. In this sense we can transform the temporal average into a spatial average problem.

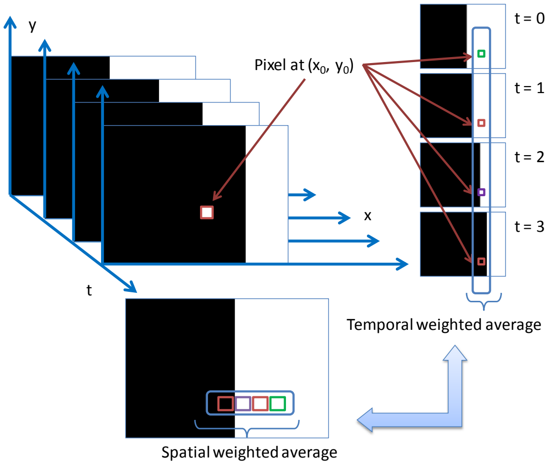

Fig. 3. Illustration spatio-temporal equivalence. To evaluate the integral in Equation (4), we first fix a position (x_0, y_0) and consider the pixel values at different times $t = 0, \ldots, 3$. The average is taken over the time, so it is the average across the four marked pixels on the right hand side. However, since these four frames are identical to each other (after motion compensation), we can evaluate the temporal average by averaging four adjacent pixels (in spatial domain).

Definition 1. *Given the velocities (v_x, v_y) and the sample-hold period T, we let $K \gg \max\{v_xT, v_yT\}$ be an integer multiple of v_xT and v_yT, and define two sequences*

$$\mathcal{S}_x = \left\{k, \; s.t. \; \frac{kv_xT}{K} \text{ is an integer, where } k \text{ is an integer}\right\},$$

$$\mathcal{S}_y = \left\{k, \; s.t. \; \frac{kv_yT}{K} \text{ is an integer, where } k \text{ is an integer}\right\}.$$

Define $\mathcal{S} = Sort\{\mathcal{S}_x, \mathcal{S}_y\} = \{k, \; s.t. \; k$ is taken from $\mathcal{S}_x$ and $\mathcal{S}_y$ and k is sorted in an acending order$\}$.

Define the weights $h(i, j)$ using the following algorithm: For every $s_k \in \mathcal{S} = \{0, s_1, \ldots, s_P\}$,

- *If $s_k \in \mathcal{S}_x$, then $i \leftarrow i+1$, and $h(i, j) = (s_k - s_{k-1})/K$,*
- *If $s_k \in \mathcal{S}_y$, then $j \leftarrow j+1$, and $h(i, j) = (s_k - s_{k-1})/K$,*
- *$h(0, 0) = s_1$.*

Definition 1 is used to characterize the discrete running index and count the repeated indices, which will become clearer when we prove the theorem. As a quick example, consider $v_xT = 3$, $v_yT = 4$, and $K = 1200$. Using Definition 1, we have $\mathcal{S}_x = \{0, 400, 800, 1200\}$ and $\mathcal{S}_y = \{0, 300, 400, 600, 900, 1200\}$. If we concatenate these two sequences and sort them, then we have $\mathcal{S} =$

$\{0, 300, 400, 600, 800, 900, 1200\}$. Thus, entries of $h(i,j)$ are

$$
\begin{aligned}
h(0,0) &= 300/1200 = 1/4,\\
h(0,1) &= (400-300)/1200 = 1/12\\
h(1,0) &= (600-400)/1200 = 1/6\\
&\vdots \;\; \vdots\\
h(2,3) &= (1200-900)/1200 = 1/4.
\end{aligned}
$$

Theorem 1. *Assume that $I_c(x,y,t) \approx I_c(x,y,t+\delta t)$ for $\delta t < T$. Let T be the sample-hold period of the liquid crystal, $K \gg \max\{v_x T, v_y T\}$ be an integer multiple of $v_x T$ and $v_y T$. Also, let M and N be the largest integer smaller than $v_x T \frac{K-1}{K}$ and $v_y T \frac{K-1}{K}$ respectively, that is*

$$
M = \left\lfloor v_x T \frac{K-1}{K} \right\rfloor \quad \textit{and} \quad N = \left\lfloor v_y T \frac{K-1}{K} \right\rfloor,
$$

where $\lfloor \cdot \rfloor$ is the floor operator. Then the integral (4) can be evaluated as

$$
\begin{aligned}
I_o^{LCD}(x,y,t) &= \frac{1}{T}\int_0^T I_c(x - v_x\tau, y - v_y\tau, t-\tau)d\tau\\
&\approx \sum_{i=0}^{M}\sum_{j=0}^{N} I_c(x-i, y-j, t)h(i,j), \qquad (5)
\end{aligned}
$$

where $h(i,j)$ is defined in Definition 1.

Proof: We first explain the assumption that $I_c(x,y,t) \approx I_c(x,y,t+\delta t)$ if $\delta t < T$. Digital video is a sequence of temporally sampled images of a continuous scene. Unless the scene contains extremely high frequency components such as a checkerboard pattern, typically the correlation between frames is high. Since no intermediate image is captured between two consecutive frames, we assume that $I_c(x,y,t) \approx I_c(x,y,t+\delta t)$ if $\delta t < T$. Other assumptions about the intermediate images are also possible, such as a linear translation from frame $I_c(x,y,t)$ to $I_c(x,y,t+T)$. But for simplicity we assume that $I_c(x,y,t)$ holds until the next sample arrives.

Using this assumption we have

$$
\begin{aligned}
I_o^{LCD}(x,y,t) &= \frac{1}{T}\int_0^T I_c(x - v_x\tau, y - v_y\tau, t-\tau)d\tau\\
\approx \frac{1}{T}&\int_0^T I_c(x - v_x\tau, y - v_y\tau, t)d\tau. \qquad (6)
\end{aligned}
$$

Let $K \gg \max\{v_x T, v_y T\}$ be an integer multiple of $v_x T$ and $v_y T$. Also, we let the finite difference interval be $\Delta\tau = \frac{T}{K}$. Then the integral in (6) can be approximated by a finite sum

$$
\begin{aligned}
I_o^{LCD}(x,y,t) &\approx \frac{1}{T}\int_0^T I_c(x - v_x\tau, y - v_y\tau, t)d\tau\\
&\approx \frac{1}{T}\sum_{k=0}^{K-1} I_c(x - v_x k\Delta\tau, y - v_y k\Delta\tau, t)\Delta\tau\\
&= \frac{1}{K}\sum_{k=0}^{K-1} I_c\left(x - k\frac{v_x T}{K}, y - k\frac{v_y T}{K}, t\right). \qquad (7)
\end{aligned}
$$

Now assume that $I_c(x,y,t)$ is a digital image at a particular time t. Since the image is composed of a finite number of pixels and each pixel has a finite size, we have $I_c(x,y,t) = I_c(x+\Delta x, y+\Delta y, t)$ if $|\Delta x| < 1$ and $|\Delta y| < 1$. Therefore, the above sum can be partitioned into groups as

$$
\begin{aligned}
I_o^{LCD}(x,y,t) &= \frac{1}{K}\sum_{k=0}^{K-1} I_c\left(x - k\frac{v_x T}{K}, y - k\frac{v_y T}{K}, t\right)\\
&= \frac{1}{K}\sum_{k=0}^{K-1} I_c\left(x - \left\lfloor k\frac{v_x T}{K}\right\rfloor, y - \left\lfloor k\frac{v_y T}{K}\right\rfloor, t\right)\\
&= \frac{1}{K}\Big[\sum_{k=0}^{s_1-1} I_c(x,y,t) + \sum_{k=s_1}^{s_2-1} I_c(x-i_{1k}, y-j_{1k}, t) + \ldots\\
&\quad + \sum_{k=s_{P-1}}^{s_P} I_c(x-i_{P-1,k}, y-j_{P-1,k}, t)\Big].
\end{aligned}
$$

where $\mathcal{S} = \{s_1, \ldots, s_P\}$ is defined by Definition 1. In each term $\sum_{k=s_p}^{s_{p+1}-1} I_c(x-i_{pk}, y-j_{pk}, t)$, the indices i_{pk} (similarly for j_{pk}) are given by

$$
i_{pk} = \begin{cases} \left\lfloor k\frac{v_x T}{K}\right\rfloor, & \text{if } s_p \in \mathcal{S}_x,\\ 0, & \text{otherwise.}\end{cases}
$$

Using the definition of $h(i,j)$ in Definition 1, we can further simplify the above expression as

$$
\begin{aligned}
&I_o^{LCD}(x,y,t)\\
&\approx \frac{1}{K}\Big[\sum_{k=0}^{s_1-1} I_c(x,y,t) + \sum_{k=s_1}^{s_2-1} I_c(x-i_{1k}, y-j_{1k}, t) + \ldots\\
&\quad + \sum_{k=s_{P-1}}^{s_P} I_c(x-i_{P-1,k}, y-j_{P-1,k}, t)\Big]\\
&= \sum_{i=0}^{M}\sum_{j=0}^{N} I_c(x-i, y-j, t)h(i,j)
\end{aligned}
$$

where $M = \left\lfloor v_x T\frac{K-1}{K}\right\rfloor$ and $N = \left\lfloor v_y T\frac{K-1}{K}\right\rfloor$. ■

As explained before, the importance of Theorem 1 is that the *temporal* problem is transformed into a *spatial* problem. Therefore, the temporal motion blur can now be treated as spatial blur problem.

C. Example

To illustrate the meaning of the parameters in Theorem 1, we show an example. Suppose that there is a diagonal motion of $v_x = 180$ pixel/sec and $v_y = 180$ pixel/sec, and let us assume that the LCD has a sample-hold period of $T = 1/60$ seconds. Since $\max\{v_x T, v_y T\} = 3$, we may define $K = 6$ (K and is an integer multiple of $\max\{v_x T, v_y T\}$). Let $k = 0, 1, 2, 3, 4, 5$, then $i = 0, 1, 2$ and $j = 0, 1, 2$ (See Definition 1), $M = 2$ and $N = 2$.

We define $S_x = \{0, 2, 4, 6\}$ and $S_y = \{0, 2, 4, 6\}$. Concatenating and sorting $\mathcal{S}_x$ and $\mathcal{S}_y$ yields $\mathcal{S} = \{0, 2, 4, 6\}$. Therefore,

- $h(0,0) = (2-0)/6 = 1/3$,
- $h(1,1) = (4-2)/6 = 1/3$,
- $h(2,2) = (6-4)/6 = 1/3$,

and $h(i, j) = 0$ for otherwise.

Thus the observed LCD signal can then be computed as

$$\begin{aligned} I_o^{LCD}(x, y, t) &\approx \sum_{i=0}^{M} \sum_{j=0}^{N} I_c(x - i, y - j, t)h(i, j) \\ &= I_c(x, y, t)h(0, 0) + I_c(x - 1, y - 1, t)h(1, 1) + \dots \\ &\quad + I_c(x - 2, y - 2, t)h(2, 2) \\ &= \frac{1}{3}[I_c(x, y, t) + I_c(x - 1, y - 1, t) + I_c(x - 2, y - 2, t)]. \end{aligned}$$

D. Discussion

There are some observations regarding Theorem 1.

First, Theorem 1 shows that although the perceived LCD blur is a temporal average, it can be approximated by a spatial average.

Second, the skewness of $h(i, j)$ is determined by the direction of the motion. If $v_x = v_y$ (as in our example), then $h(i, j)$ becomes diagonal; If $v_x = 0$, then $h(i, j)$ becomes vertical; If $v_y = 0$, then $h(i, j)$ becomes horizontal. In these three special cases, all the non-zero entries of $h(i, j)$ are identical. If the motion direction is not horizontal, vertical or diagonal, then an entry of $h(i, j)$ is larger if the distance between the line along the motion direction and (i, j) is closer.

Third, magnitude of the motion determines the length of the filter $h(i, j)$, hence the blurriness of the perceived image. If there is no motion, then $h(i, j) = 1$ and so there will be no blur. However, if the motion is large, then $h(i, j)$ will be long and so the averaging effect will be strong.

Fourth, compared to a 60Hz LCD monitor, a 240Hz LCD monitor shows better perceptual quality because it refreshes 4 times faster than a 60Hz monitor. This effect can be reflected by reducing the sample-hold period T and hence the length of the filter $h(i, j)$.

E. Numerical Implementation of Theorem 1

Algorithm 1 Compute $h(i, j)$ and $I_o^{LCD}(x, y, t)$

```
Fix a time instant $t$, and LCD decay time $T$.
Step 1: Use motion estimation algorithm to detect $(v_x, v_y)$.
Step 2: Define weights $h(i, j)$ according to Definition 1.
Step 3: Set $h(i, j) = 0$, if $i > L$ or $j > L$ for some $L$ (to be discussed in Section III).
Step 4: Compute $I_o^{LCD}(x, y, t)$ using via discrete convolution in Equation (5).
```

Algorithm 1 is a pseudocode for numerical implementation of Theorem 1. The algorithm consists of four steps. In the first step, motion vectors are computed using methods such as full search, three step search [26], directional methods [27], or hybrid methods [28]. The second step is to define the blur kernel $h(i, j)$ according to definition (1). Note that each $h(i, j)$ is defined locally, meaning that one motion vector defines one $h(i, j)$. If there is a collection of motion vectors, then correspondingly there will be a collection of $h(i, j)$. In step 3, $h(i, j)$ is limited to a finite length and width for modeling the eye tracking property, which will be discussed in Section III. Last, the output can be computed via a discrete convolution shown in Equation (5).

F. Comparison between Spatial and Temporal Integration

To verify Theorem 1, we compare the temporal integration (Equation (4)) and spatial integration (Equation (5)) using simulations. Our simulation methodology follows from [29], where the authors show that the simulation is a good substitute for a comprehensive experiment to measure liquid crystals response.

Fig. 4 shows four simulation results [2]. For each video sequence, two consecutive frames are collected, and the relative motion is computed using a full search algorithm [26]. 10 motion compensated frames are inserted via standard H.264 motion compensation algorithm. This is to simulate a continuous time signal. The temporal integration is calculated as the average of the 10 motion compensated frames.

To measure the difference between spatial integration and the temporal integration, PSNR values are computed. As shown, on average the PSNR is higher than 40dB, which implies a small difference between the two methods. However, the computing time using the spatial approximation is significantly shorter than the temporal integration (we used a 10× frame rate up conversion by linear interpolation).

TABLE I
COMPARISON BETWEEN SPATIAL INTEGRATION AND TEMPORAL INTEGRATION. MAXIMUM MV REFERS TO THE MAXIMUM MOTION VECTOR IN THE IMAGE. PSNR MEASURES THE DIFFERENCE BETWEEN THE SPATIAL INTEGRATION TO THE TEMPORAL INTEGRATION. HIGHER PSNR IMPLIES SMALLER DIFFERENCE.

Image	Size	Maximum MV	PSNR
A	200 × 200	4.35	42.45dB
B	640 × 480	3.71	41.34dB
C	320 × 240	7.23	41.10dB
D	300 × 600	10	40.81dB

III. EYE MOVEMENT LIMIT

In section II, we assume that our eye tracking system is perfect, i.e., we can track moving objects at any speed. This assumption makes the derivation simpler, but it is not true in reality. A more realistic model is that our eyes have a speed limit. We provide supports to this argument, through the literature in cognitive science and visual subjective tests.

A. Eye Tracking

In Rayner's review [30] on eye tracking system, he mentions that when we look at a scene, our eyes are rapidly moving. The rapid movement is known as the saccades, which can be as high as 500 degrees per second. However, at such a high speed we can hardly see any visual content. This phenomenon is known as the saccade suppression [31], [32]. So most of the images perceived are obtained during a period of time (typically about 200-300 ms) between saccades. This period

[2] Complete set of videos are available online at http://videoprocessing.ucsd.edu/∼stanleychan

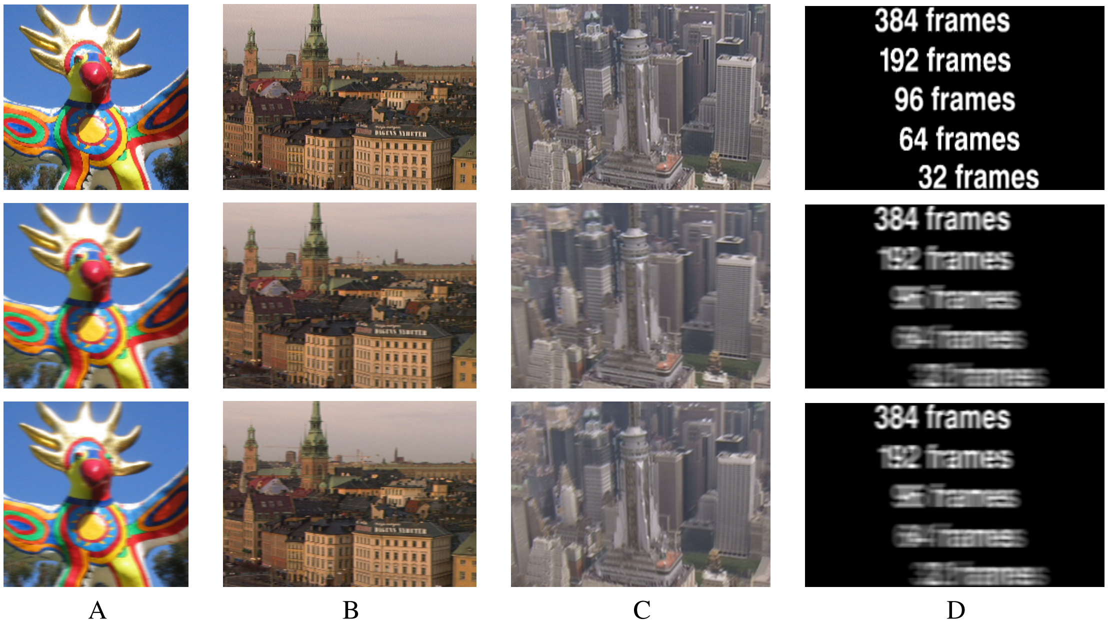

Fig. 4. Simulation results of spatial and temporal integration. Top row: original input image; middle row: simulated blur using spatial integration; bottom row: simulated blur using temporal integration.

is known as the fixation. If an object is moving quickly, then the duration of fixation is shortened, and hence the perceptual quality reduces. Therefore, even if our eyes may be able to *track* an object, we may not be able to *see* what it is.

The relation between object speed and perceived sharpness can be concluded from the following findings.

1) Westerink and Teunissen [33] conducted two experiments about the relation between perceptual sharpness and the picture speed. In their first experiment, they asked the viewers to track a moving image with their heads stay at a fixed position (referred to as the fixation condition). The conclusion is that the perceived sharpness drops to a minimum score when picture speed is beyond 5 deg/s (See Fig. 4 of [33]). A similar conclusion can also be drawn from [34].
2) In the second experiment by Westerink and Teunissen [33], viewers were allowed to move their heads (referred to as the pursuit condition). The conclusion is that the perceived sharpness drops to a minimum score when picture speed is beyond 35 deg/s (See Fig. 6 of [33]).
3) Bonse [35] studied a mathematical model for temporal subsampling. They mentioned that there is a maximum eye tracking velocity of 5 to 50 deg/s, which had been experimentally justified by Miller and Ludvigh [36].
4) Glenn and Glenn [37] studied the discrimination of human eyes on televised moving images of high resolution (300-line) and low resolution (150-line). Their results show that it is harder for human eye to discriminate high resolution from low resolution images if the speed increases.
5) Gegenfurtner [38] studied the relation between pursuit eye movement and perceptual performance. The viewers were asked to track a moving image of speed 4 deg/s. Results show that the recorded the eye velocities are ranged between 3 deg/s to 4.5 deg/s.

The conclusion of these findings is that when picture motion increases, the perceptual sharpness decreases. In some experiments, the maximum picture speed is found to be 5 deg/s for fixation condition, and 35 deg/s for pursuit condition. Beyond this threshold, our eyes are unable to capture visual content from the image.

B. LCD Model with Eye Tracking

The existence of the maximum eye tracking speed implies that the LCD model has to be written as

$$\begin{aligned} I_m(x,y,t) &= I_s(x-u_xt, y-u_yt, t) \\ &= \int_0^T h_D(\tau) I_c(x-v_x\tau-(u_x-v_x)t, \ldots \\ &\quad y-v_y\tau-(u_x-v_x)t, t-\tau)d\tau. \end{aligned}$$

where u_x and u_y are the eye tracking speed. If the picture speed is low, then our eyes are able to capture the visual content, and hence $u_x = v_x$ and $u_y = v_y$. However, if the picture speed is beyond the threshold, then the difference $(u_x - v_x)\tau$ accounts for the images that we cannot see.

Consequently, we apply this observation to design inverse filters to reduce LCD motion blur. Previous efforts in inverse filter design for LCD motion blur can be found in [15], [17] and [39]. In these papers, the inverse filter is designed according to the estimated point spread function $h(i,j)$. If $h(i,j)$ has a narrow frequency support, then noise in an image will be amplified by the inverse filter.

Due to the presence of the maximum eye tracking speed, we know that fast moving objects cannot be seen clearly. Therefore, a natural question is that whether it is necessary to construct a very long $h(i,j)$ and let its inverse filter to

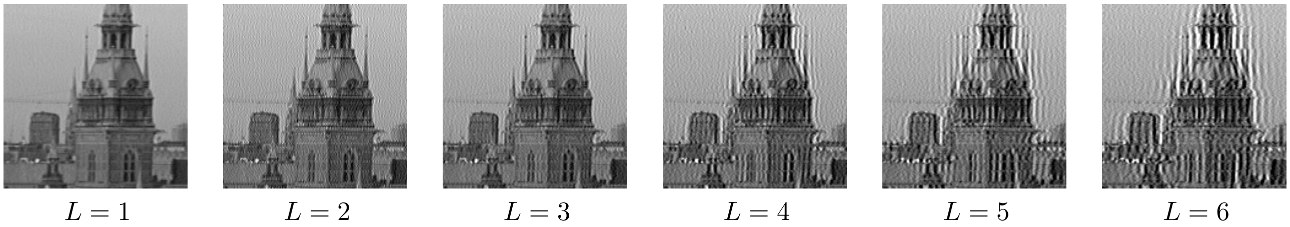

Fig. 5. Video 2 Stockholm. The sequence is processed using [39], with different values of L.

introduce flickering artifacts. To this end, we find that it is more appropriate to limit the size of $h(i, j)$ as

$$h(i,j) = \begin{cases} h(i,j), & \text{if } i \leq L \text{ and } j \leq L, \\ 0 & \text{else }, \end{cases}$$

where L denotes the maximum number of pixels along the horizontal and vertical direction. For example, $L = 4$ means that the size of $h(i, j)$ is at most 4×4 pixels.

The exact value of L is difficult to determine as it depends on a number of factors such as the conditions of 5 deg/s for fixation and 35 deg/s for pursuit. To compromise this issue we seek a method to estimate a value of L so that it can be used for our deblurring algorithm, which will be described next.

C. Experiments

To determine the maximum length of the filter $h(i, j)$ we performed a visual subjective test.

Three video sequences are used in this test, where each video sequence consists of a global horizontal motion. The motion vectors are determined by full search algorithm and the point spread function $h(i, j)$ is found using Algorithm 1. In order to determine the maximum length L for $h(i, j)$, we truncate $h(i, j)$ using 6 different values of L. For each L, we over-sharpen the video sequence by using the optimization approach presented in [39]. The optimization problem is solved using a conjugate gradient algorithm (LSQR [40]), with damping constant $\lambda = 1e^{-1}$. Maximum number of iterations is set to be 100, and tolerance level is set to be $1e^{-6}$.

Fig. 5 shows the results. When L increases, it can be observed that more artifacts are introduced. To quantify the amount of artifacts, we calculate the average total variation around neighborhood pixels:

$$e = \Big(\frac{1}{MN} \sum_{i,j} |f(i+1,j) - f(i,j)|^2 + |f(i,j+1) - f(i,j)|^2 \Big)^{1/2}, \tag{8}$$

where $f(i, j)$ is the image under consideration, and M and N are the number of columns and rows of $f(i, j)$.

TABLE II
AVERAGE TOTAL VARIATION ERROR (DEFINED IN EQUATION (8)) AROUND ADJACENT PIXELS.

L	Video 1 Shield	Video 2 Stockholm	Video 3 Black White
1	0.0465	0.0546	0.0478
2	0.0589	0.0764	0.0504
3	0.0655	0.0895	0.0533
4	0.0896	0.1205	0.0608
5	0.1010	0.1279	0.0581
6	0.1146	0.1412	0.0620

TABLE III
THE SUBJECTIVE TESTS TO DETERMINE THE MAXIMUM LENGTH L.

Subjective Test to determine optimal L			
	Video 1 Shield	Video 2 Stockholm	Video 3 Black White
mean	4.19	3.89	3.39
std	0.67	0.65	0.90

The visual subjective test procedure follows from ITU-R BT. 1082, Section 8 [41]. 18 human viewers were invited to the experiment. For each of the three video sequences, there are six levels of the maximum lengths ($L = 1, \ldots, 6$). $L = 1$ means that $h(i, j)$ is a delta function, which in turn implies that there is no inverse filtering. $L = 6$ means that $h(i, j)$ has a size of 6×6, and so there is a substantial inverse filtering. Each time the viewers were presented a reference and a processed video sequence simultaneously. They were asked to tell whether the processed one showed any distracting artifacts. If they replied no, then L would be increased until the level such that noise became appealing. The videos were played on a PC with 2.8GHz CPU, 8GB DDR2 RAM, ATI Radeon 2600 XT 512MB video card. The video sequences were uncompressed, played at 60 frames per second.

The mean and variance of L is shown in Table III. It can be observed that if we limit the size of the point spread function $h(i, j)$ to 4×4 (on average) and apply the conjugate gradient algorithm to deblur the image, viewers can perceive the maximum degree of sharpness before they notice artifacts.

A limitation of this experiment is that it relies on the formulation in [39]. If other formulations such as the spatial and temporal regularization functions (See Section IV) are used, the maximum length L can possibly be increased as artifacts can be suppressed more using these methods.

IV. DEBLURRING ALGORITHM

The objective of this section is to propose a deblurring algorithm for LCD motion blur reduction.

A. Optimization Formulation

First, by spatio-temporal equivalence (Equation (5)), we know that the observed (blurred) image is related to the original (sharp) image by a linear convolution. Therefore, we can apply the standard imaging model (see, e.g., [42]) to model the image formation as

$$\mathbf{g} = \mathbf{H}\mathbf{f} + \eta, \tag{9}$$

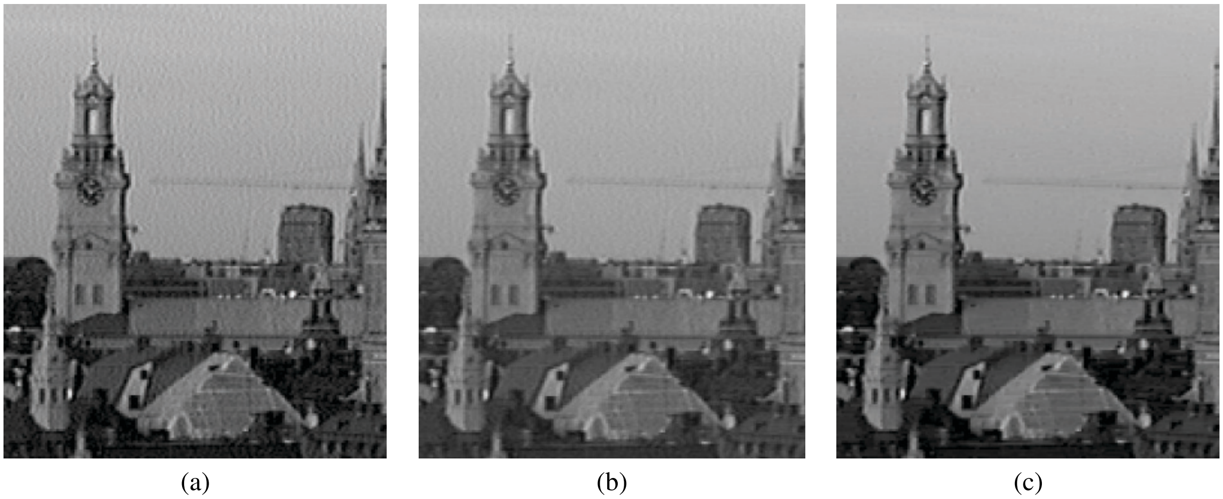

Fig. 6. Comparison between various regularization functions. (a) Solution obtained by minimizing $\|\mathbf{Hf}-\mathbf{g}\|_2^2$. (b) Solution obtained by Tikhonov $\|\mathbf{Hf}-\mathbf{g}\|_2^2+\lambda\|\mathbf{D_x f}\|_2^2$, where $\lambda = 0.0005$. (c) Solution obtained by minimizing the proposed method $\|\mathbf{Hf}-\mathbf{g}\|_2^2+\lambda\|\mathbf{D_x f}\|_1$, where $\lambda = 0.0015$.

where $\mathbf{f} = \mathrm{vec}[f(x,y)]$ and $\mathbf{g} = \mathrm{vec}[g(x,y)]$ are vectors that denote the sharp image $f(x,y)$ and the observed (blurred) images $g(x,y)$ respectively. Here, $\mathrm{vec}(\cdot)$ is the vectorization operator which stacks an image into a long column vector according to the lexicographical order. $\mathbf{H}$ is a block circulant matrix denoting the blurring (convolution) operator, and η is an additive noise term.

The LCD deblurring problem may be formulated within an optimization framework by considering the least-squares minimization problem

$$\begin{aligned} \underset{\mathbf{f}}{\text{minimize}} \quad & \|\mathbf{Hf}-\mathbf{g}\|_2^2 \\ \text{subject to} \quad & 0 \le \mathbf{f} \le 1. \end{aligned} \tag{10}$$

where $\|\cdot\|_2$ denotes the l_2-norm. The choice of l_2 norm is based on the assumption that the noise η is Gaussian. The bounds on the optimization variable $\mathbf{f}$ is to ensure that a pixel value does not exceed the range of $[0,\ 255]$, or $[0,\ 1]$ in the normalized scale.

Problem (10) is ill-posed because the operator $\mathbf{H}$ often has a large condition number. Therefore, in the presence of noise, solving (10) may lead to undesirable images. To resolve this issue, the standard method is to introduce a regularization function $\mathbf{R}_{\text{reg}}(\mathbf{f})$ and solve

$$\begin{aligned} \underset{\mathbf{f}}{\text{minimize}} \quad & \|\mathbf{Hf}-\mathbf{g}\|_2^2 + \lambda \mathbf{R}_{\text{reg}}(\mathbf{f}) \\ \text{subject to} \quad & 0 \le \mathbf{f} \le 1. \end{aligned} \tag{11}$$

In statistics, the regularization is also known as the prior information about the image. The constant λ is a regularization parameter that weights the objective function relative to the regularization term.

B. Spatial Regularization

The spatial regularization function is defined by the gradients of the image. Specifically, we define the directional gradient operators $\mathbf{D}_x$, $\mathbf{D}_y$, $\mathbf{D}_{d1}$ and $\mathbf{D}_{d2}$ as

$$\begin{aligned} \mathbf{D}_x\mathbf{f} &= \mathrm{vec}[f(x+1,y)-f(x,y)] \\ \mathbf{D}_y\mathbf{f} &= \mathrm{vec}[f(x,y+1)-f(x,y)] \\ \mathbf{D}_{d1}\mathbf{f} &= \mathrm{vec}[f(x-1,y+1)-f(x,y)] \\ \mathbf{D}_{d2}\mathbf{f} &= \mathrm{vec}[f(x+1,y+1)-f(x,y)], \end{aligned}$$

where $\mathbf{f} = \mathrm{vec}[f(x,y)]$ is the unknown image, $\mathbf{D}_x$ and $\mathbf{D}_y$ represent the directional derivative operators along the horizontal and vertical directions respectively, and $\mathbf{D}_{d_1}$ and $\mathbf{D}_{d_2}$ represent the directional derivative operators along the direction from top left to bottom right and from top right to bottom left respectively. The transposes of these operators are

$$\begin{aligned} \mathbf{D}_x^T\mathbf{f} &= \mathrm{vec}[f(x-1,y)-f(x,y)] \\ \mathbf{D}_y^T\mathbf{f} &= \mathrm{vec}[f(x,y-1)-f(x,y)] \\ \mathbf{D}_{d1}^T\mathbf{f} &= \mathrm{vec}[f(x+1,y-1)-f(x,y)] \\ \mathbf{D}_{d2}^T\mathbf{f} &= \mathrm{vec}[f(x-1,y-1)-f(x,y)]. \end{aligned}$$

The spatial regularization function is defined as

$$\mathbf{R}_S(\mathbf{f}) = \sum_i \|\mathbf{D}_i\mathbf{f}\|_1, \tag{12}$$

where the subscript $i \in \{x,\ y,\ d_1,\ d_2\}$ represents the direction. This spatial regularization is a special case of the bilateral total variation introduced by Farsiu, Robinson, Elad and Milanfar [43], [44], [45]. It can also be considered as an l_1 approximation to the conventional total variation (TV) regularization introduced by Rudin, Osher and Fatemi [46]. In [25], Yao et al used a regularization function similar to ours for the application of removing coding artifacts.

The advantage of using the proposed spatial regularization over the conventional Tikhonov regularization $\mathbf{R}(\mathbf{f}) = \|\mathbf{D}_x\mathbf{f}\|^2 + \|\mathbf{D}_y\mathbf{f}\|^2$ is that Tikhonov regularization cannot preserve sharp edges. Fig. 6 shows some comparisons between the proposed spatial regularization and Tikhonov regularization. Detailed discussions can be found in [47] and [48].

C. Temporal Regularization

Although the spatial regularization function can be applied to each frame of a video individually, the temporal consistency of the video is not guaranteed. Temporal consistency describes whether two adjacent frames have a smooth transition. If a pixel has a sudden increase/decrease in brightness along the time axis, then it is said to have temporal inconsistency. As an illustration, two consecutive frames taken from a real video are shown in Fig. 7. Note that pixels around the edges of the window have different intensities in the two adjacent frames, although they are at the same location.

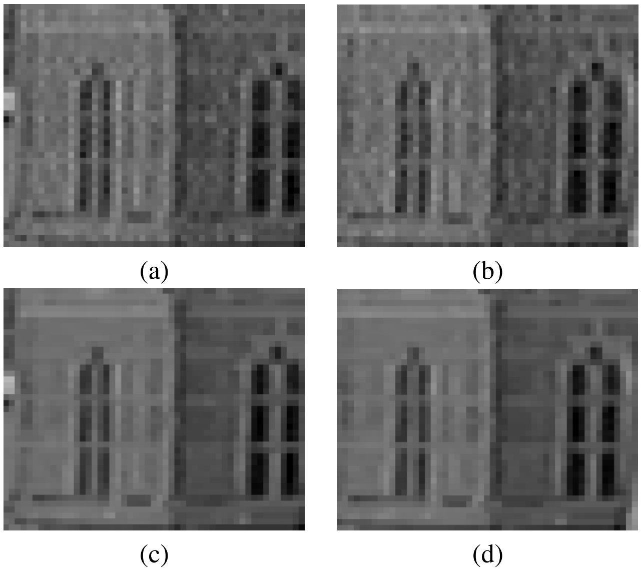

Fig. 7. Two consecutive frames. (a)-(b): No temporal regularization. (c)-(d): With temporal regularization.

To enhance the temporal consistency we introduce a regularization function along the temporal direction. A similar approach was previously used by Yao et al for denoising [25]. The temporal regularization function is defined as

$$\mathbf{R}_T(\mathbf{f}) = \|\mathbf{f} - \mathbf{M}\mathbf{f}_0\|_2^2,$$

where $\mathbf{M}$ is a geometric wrap (i.e., motion compensation), and $\mathbf{f}_0$ is the solution of the previous frame. The interpretation of $\mathbf{R}_T(\mathbf{f})$ is that the current solution should be close to the previous solution after motion compensation. Thus, by minimizing $\mathbf{R}_T(\mathbf{f})$, we can reduce the temporal noise.

The effectiveness of the proposed temporal regularization function can be seen in Fig. 7. Fig. 7(a)-(b) show two consecutive frames without temporal regularization, where as 7(c)-(d) show two consecutive frames with temporal regularization. It can be observed that the transition of pixel values is smoother in (c)-(d) than (a)-(b).

D. Convolution Operator $\mathbf{H}$

The convolution operator $\mathbf{H}$ is constructed based on the motion vectors. If the motion is global, then $\mathbf{H}$ corresponds to a spatially invariant point spread function. In this case, $\mathbf{H}$ is a block-circulant-with-circulant-block (BCCB) matrix [49], and it can be diagonalized by Fourier Transforms [50]. As a result, computation of the matrix-vector product $\mathbf{H}\mathbf{f}$ can be performed in $O(n \log n)$ operations, where n is the number of pixels.

For general video sequences, the motion is not global and so $\mathbf{H}$ does not correspond to a spatially invariant point spread function. In the worst case where every pixel has a different motion, each pixel will have a different point spread function. Because of that, $\mathbf{H}$ do not have the BCCB structure and so it cannot be diagonalized by Fourier Transforms. Hence, to compute the matrix-vector multiplication $\mathbf{H}\mathbf{f}$, one has to do it in the spatial domain directly. The complexity is in the order of $O(nk)$, where n is the number of image pixels, and k is the number of pixels of the largest point spread function.

Since the motion is not global in general, many existing algorithms cannot be used as they assume $\mathbf{H}$ to a BCCB matrix. These methods include the half quadratic penalty methods by Huang et al [51], Wang et al [52], Geman, Yang and Reynolds [53], [54] and Yao et al [25], the interior point method by Nesterov [55] and the projected gradients methods by Chambolle [56]. In the followings, we present a method that supports both BCCB matrices and general matrices.

E. Subgradient Projection Algorithm

The overall optimization problem is

$$\begin{aligned} &\underset{\mathbf{f}}{\text{minimize}} \quad \|\mathbf{H}\mathbf{f} - \mathbf{g}\|_2^2 + \lambda \sum_i \|\mathbf{D}_i\mathbf{f}\|_1 + \gamma\|\mathbf{f} - \mathbf{M}\mathbf{f}_0\|_2^2 \\ &\text{subject to} \quad 0 \le \mathbf{f} \le 1, \end{aligned} \tag{13}$$

where λ and γ are two regularization parameters.

Subgradient projection is a variation of the steepest descent algorithm. Given the k^{th} iterate, the algorithm updates the $k+1^{th}$ iterate by

$$\begin{aligned} \mathbf{f}^{k+1} = \mathbf{f}^k - \alpha_k \nabla\Big(&\|\mathbf{H}\mathbf{f}^k - \mathbf{g}\|_2^2 + \dots \\ &+ \lambda \sum_i \|\mathbf{D}_i\mathbf{f}^k\|_1 + \gamma\|\mathbf{f}^k - \mathbf{M}\mathbf{f}_0\|_2^2\Big), \end{aligned}$$

where α_k is the step size, and $\nabla(\cdot)$ is the gradient operator. Since the l_1 term is not differentiable, we consider its subgradient instead of the gradient. The (sub)gradients of individual terms are

$$\nabla\left(\|\mathbf{H}\mathbf{f} - \mathbf{g}\|_2^2\right) = 2\mathbf{H}^T(\mathbf{H}\mathbf{f} - \mathbf{g}) \tag{14}$$

$$\nabla\left(\sum_i \|\mathbf{D}_i\mathbf{f}\|_1\right) = \sum_i \mathbf{D}_i^T \text{sgn}(\mathbf{D}_i\mathbf{f}) \tag{15}$$

$$\nabla\left(\|\mathbf{f} - \mathbf{M}\mathbf{f}_0\|_2^2\right) = 2(\mathbf{f} - \mathbf{M}\mathbf{f}_0), \tag{16}$$

where $\text{sgn}(x) = 1$ if $x > 0$, -1 if $x < 0$ and 0 if $x = 0$.

The simple bound constraints can be handled by projecting out-of-bound components to their closest bounds. In other words, we set

$$[\mathbf{f}]_i = \begin{cases} 1, & \text{if } [\mathbf{f}]_i \ge 1, \\ 0, & \text{if } [\mathbf{f}]_i \le 0. \end{cases} \tag{17}$$

where $[\cdot]_i$ denotes the i^{th} component of $\mathbf{f}$.

The step size is chosen to satisfy the "square summable but not summable" rule (see, e.g., [57], [58], [59]):

$$\sum_{k=0}^{\infty} \alpha_k^2 < \infty \quad \text{and} \quad \sum_{k=0}^{\infty} \alpha_k = \infty.$$

In our problem, we choose $\alpha_k = M/(M+k)$, for some maximum number of iterations M, typically $M = 1000$.

We also implemented the Armijo line search algorithm [60], [61]. For fixed constants $0 < \eta < 1$, and $0 < \rho < 1$, we let $\Phi(\mathbf{f}) = \|\mathbf{Hf} - \mathbf{g}\|_2^2 + \lambda \sum_i \|\mathbf{D}_i\mathbf{f}\|_1 + \gamma\|\mathbf{f} - \mathbf{Mf}_0\|_2^2$. If $\Phi(\mathbf{f}^{k+1}) - \Phi(\mathbf{f}^k) \leq \alpha\eta\|\nabla\Phi(\mathbf{f}^k))\|_2^2$, then the step size α is reduced by $\alpha \leftarrow \rho\alpha$, until the condition is satisfied.

In theory, subgradient projection algorithm with the square summable rule has provable convergence, [57], [59]. But in practice, if we allow the algorithm to terminate early, then the Armijo line search algorithm often gives better PSNR than square summable rule.

Algorithm 2 shows the pseudo-code for our projected subgradient algorithm using the Armijo line search.

Algorithm 2 Subgradient Projection Algorithm

```
Set $\lambda$ and $\gamma$ (Typically, $\lambda \approx 0.0015$, $\gamma \approx 0.1$).
Set initial step size $\alpha_k = 1$.
Initialize variables.
while $k \leq k_{max}$ do
    Compute the gradients $\nabla\Phi(\mathbf{f})$ as defined in (14) - (16).
    Armijo Line Search to determine step size $\alpha$.
    Update $\mathbf{f}^{k+1} = \mathbf{f}^k - \alpha\nabla\Phi(\mathbf{f}^k)$
    $\mathbf{f}^{k+1} = \begin{cases} 1 & \text{if } \mathbf{f}^{k+1} > 1 \\ 0 & \text{if } \mathbf{f}^{k+1} < 0 \end{cases}$
    $k \leftarrow k + 1$
end while
```

Regarding the regularization parameters λ and γ, Bertsekas [58] mentioned that these parameters can never be known prior to solving the problem. There are some methods to estimate the parameters, such as generalized cross validations by Nguyen, Golub and Milanfar [62], or the $L-$ curve criteria discussed in Hansen's book [63]. But these methods are not guaranteed to work for the non-differentiable l_1 term. Therefore, in this paper we test the images with a sequence of λ and γ, and choose the ones that balance PSNR, run time, and perceptual quality. In a fully automated settings, an updating strategy based on a non-reference metric [64] can be used.

F. Experiments

In this section we compare the performance of the proposed spatio-temporal deblurring algorithm versus existing algorithms. In particular we measure three quantities of the deblurred signal.

1) Mean Square Error: The first quantity is the peak signal to noise ratio (PSNR), which is defined as

$$PSNR = 10 \log_{10} \frac{1}{MSE},$$

Here, MSE is the mean square error, defined as

$$MSE = \frac{1}{MN}\|\mathbf{Hf} - \mathbf{g}\|_2^2,$$

where M, N are the number of rows and columns of the image, and $\mathbf{f}$ is the minimization solution. PSNR measures the solution fidelity, and higher PSNR implies that the difference between $\mathbf{Hf}$ and $\mathbf{g}$ is smaller.

2) Spatial Consistency: Spatial consistency is a qualitative measurement of the deviation between neighborhood pixels. To quantify the spatial consistency we define

$$E_S = \sum_i \|\mathbf{D}_i\mathbf{f}\|_1.$$

This quantity measures the total variation of the solution $\mathbf{f}$. If E_S is large, then it is likely that $\mathbf{f}$ is noisy.

3) Temporal Consistency: Temporal consistency describes the smoothness of the video along the time axis. Given two consecutive frames $\mathbf{f}_{t+1}$, $\mathbf{f}_t$, and the motion vector field, we define

$$E_T = \|\mathbf{f}_{t+1} - \mathbf{M}_t\mathbf{f}_t\|_2^2,$$

where $\mathbf{M}_t$ is a geometric warping operator such that $\mathbf{M}_t\mathbf{f}_t$ is the motion compensated frame with respect to $\mathbf{f}_{t+1}$.

4) Results: We ran two experiments, both are panning camera scenes. The videos have global horizontal motion blur, with some small local motions.

The specification of the video is as follows: The size is 640×480 and it is stored as a sequence of 8-bit gray scaled bit maps so each pixel has a dynamic range of 256 levels. For better numerical stability we normalize the image by dividing the pixel values by 255. The video is supposed to be played at 60 fps, with 300 frames in total. We ran our experiment on a PC with AMD Dual Core 3 GHz, 8GB RAM, Radeon-HD2600XT graphics card, Windows XP-64 OS.

The results are shown in Fig. 8 and 9. The upper row of the figures show the signals synthesized by different methods, namely MCIF [15], LR [17] and the proposed method. As shown, the synthesized signals of MCIF and LR contain a lot of noise. These noise are often inconsistent in time, and so when the images are moving, viewers will see flickering artifacts. In contrast, the proposed method controls the amount of noise, both spatially and temporally. Flickering is suppressed significantly.

The lower row of the figures show the simulated images that an viewer would see. We emphasize that these are simulated images because the actual images formed on the retina of a viewer are never accessible. To simulate the observed signal, we apply $\mathbf{H}$ to the synthesized signal $\mathbf{f}$.

Numerical results using PSNR, E_S and E_T are given in Table IV. Although the proposed method does not have a PSNR as high as Lucy Richardson, it shows a 2dB improvement to the original input images. More important observations are the spatial consistency and the temporal consistency: the proposed method yields significantly lower error than the other two methods.

It should be noted that although our regularization functions has a better performance than existing methods in preserving edges, suppressing noise and enhancing temporal consistency, restoration of texture areas is still challenging. In areas where the magnitude of texture gradient is comparable to the magnitude of noise gradient, our current algorithm has limited

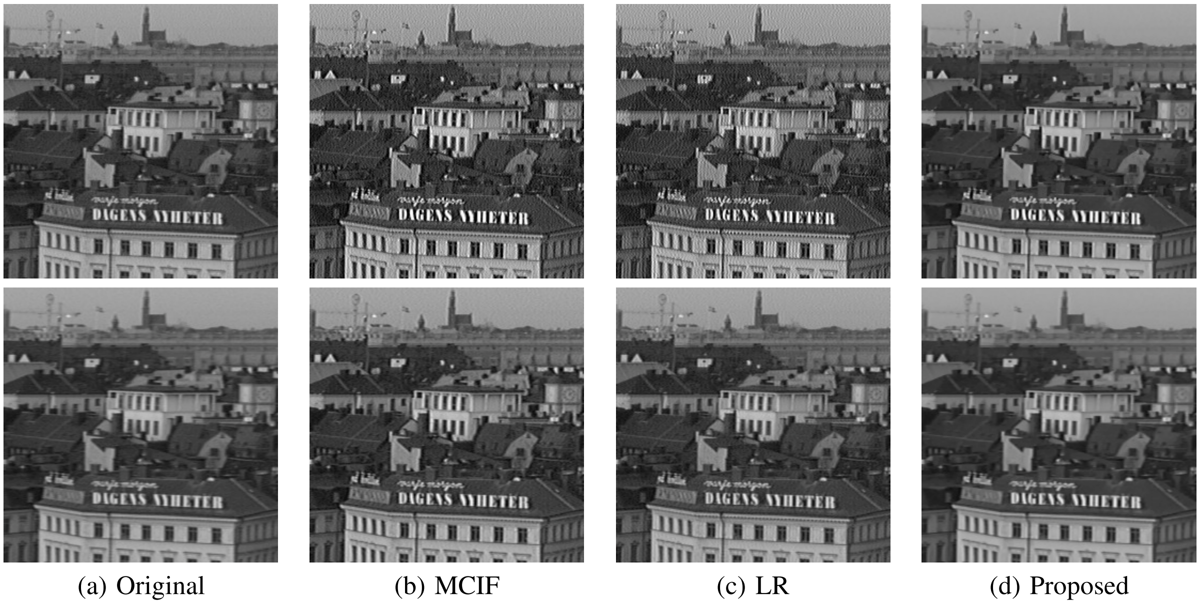
(a) Original (b) MCIF (c) LR (d) Proposed

Fig. 8. Experiment 1: The upper row shows the synthesized signal that is sent to the LCD. The lower row shows the (simulated) perceived LCD signal. (a) Original Signal (b) Signal synthesized by MCIF [15], (c) Signal synthesized by Lucy Richardson [17], (d) Signal synthesized by proposed method.

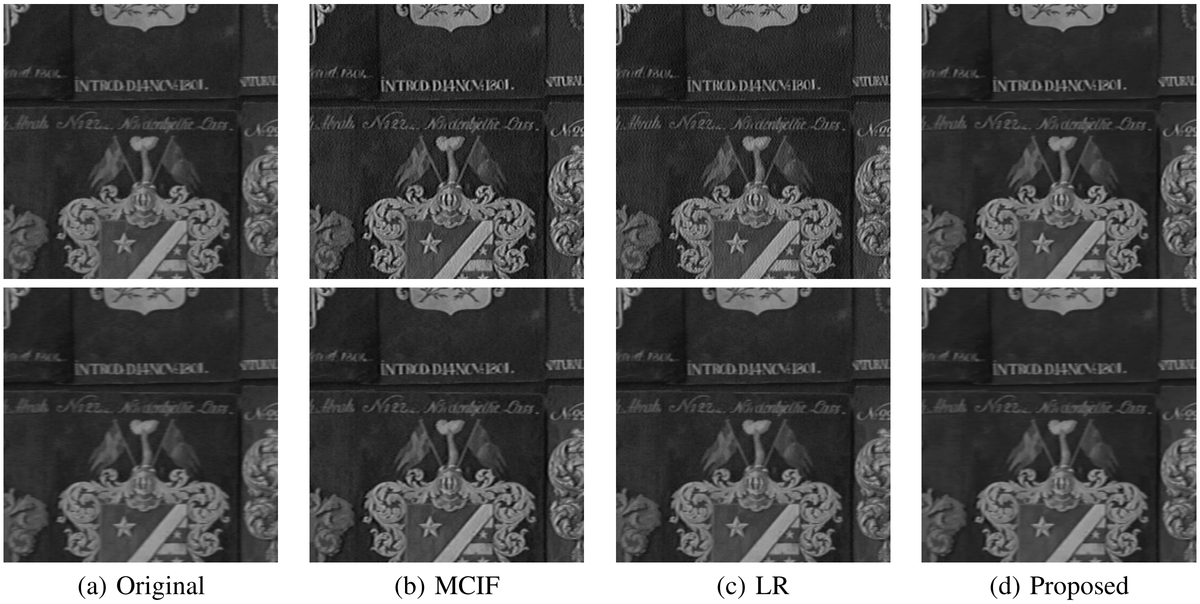
(a) Original (b) MCIF (c) LR (d) Proposed

Fig. 9. Experiment 2: The upper row shows the synthesized signal that is sent to the LCD. The lower row shows the (simulated) perceived LCD signal. (a) Original Signal (b) Signal synthesized by MCIF [15], (c) Signal synthesized by Lucy Richardson [17], (d) Signal synthesized by proposed method.

TABLE IV
COMPARISONS BETWEEN MCIF, LUCY RICHARDSON AND PROPOSED METHOD

Video Name	Methods	Signal to Noise Ratio PSNR (dB)	Spatial Error $\sum_i \|\mathbf{D}_i\mathbf{f}\|_1$	Temporal Error $\|\mathbf{f}_{t+1} - \mathbf{M}_t\mathbf{f}_t\|_2^2$
Stockholm	Original	34.43	4.8286×10^3	3.2969×10^1
	MC Inverse Filter [15]	34.357	9.8488×10^3	4.3412×10^2
	Lucy Richardson [17]	40.35	1.0914×10^4	5.5423×10^3
	Proposed Method	36.38	4.1443×10^3	3.3400×10^1
Shield	Original	36.879	3.586×10^3	7.0169×10^2
	MC Inverse Filter [15]	36.943	7.432×10^3	1.275×10^3
	Lucy Richardson [17]	48.241	7.825×10^3	1.111×10^3
	Proposed Method	38.540	3.437×10^3	8.224×10^2

performance in removing the noise while keeping the texture. Our future research is to develop methods to restore texture areas.

G. Visual Subjective Test

We ran a visual subjective test to verify our results. The subjective test is based on the single stimulus non-categorical judgement method described in ITU-R BT.500-11 [65]. In this test, 11 human viewers were invited to compare the MCIF, LR and the proposed method on the picture quality improvement of Stockholm and Shield sequences. For each test, viewers were asked to compare the original and the processed sequence on separate sides of the screen. Viewers then gave a score on a continuous scale to indicate whether one image was "much better", "better", "slightly better" or "the same" as the other image. We used a 24-inch Samsung 730B LCD with 8ms response time.

Table V shows the average and standard deviation of the subjective test scores. In the table, the average scores are all positive, meaning that the method improves the perceptual quality when compared to the original sequence. Additionally, magnitude of the average scores using the proposed method is the highest among the three methods, which implies that viewers ranked the proposed method as the best result among the three methods.

TABLE V
SUBJECTIVE TEST RESULTS OF MCIF, LR AND THE PROPOSED METHOD

		average score (μ)	std dev (σ)
Stockholm	MCIF	0.818	1.055
	Lucy Richardson	1.54	0.415
	Proposed	1.86	0.674
Shield	MCIF	0.845	0.884
	Lucy Richardson	0.954	0.723
	Proposed	1.091	0.701

In order to test the statistical significance of the perceptual testing results we employ the students t-test, where the null hypothesis is that the average score is $\mu = 0$, i.e., the proposed algorithm has no positive effect over the original sequence. If we let the confidence interval $\alpha = 0.01$, then the rejection region is $\mu \geq 2.359\sigma/\sqrt{N}$, where μ is the average score, σ is the standard deviation, and N is the number of viewers. It can be shown that the value $2.359\sigma/\sqrt{N}$ of MCIF, LR and the proposed method are 0.6406, 0.2528, 0.4105 respectively for Stockholm, and 0.5384, 0.4404, 0.4270 respectively for Shield. Since all μ are greater than these figures, we conclude that all three methods give improvements to the original sequence . In addition, it can be shown that for the proposed method, the gap between the average score and the lower bound is larger than that of the other two methods. This implies that statistically the proposed method gives a more positive effect to the original sequence than the other two methods.

V. Conclusion

This paper has three contributions. First, we proved the equivalence between temporal and spatial integration. The equivalence allows us to simulate the LCD blur efficiently in the spatial domain, instead of a time consuming integration in the temporal domain. Experiments verified that computing the LCD motion blur in the spatial domain is as accurate as computing it in the temporal domain. Second, we studied the limit of eye movement speed. Based on a number of papers in the cognitive science literature, we showed that perceptual quality reduces as picture motion increases. Beyond certain speed limit, human eyes cannot retrieve any useful content from the picture. Consequently, we showed the size of the LCD motion blur filter should be limited, and the optimal size can be determined using a visual subjective test. Third, we proposed an optimization framework to pre-process the LCD signal so that it can compensate the motion blur. In order to maintain the spatial and temporal consistencies, we introduced an l_1-norm regularization function on the directional derivatives and a l_2-norm regularization function on difference between current and previous solution. Experimental results showed that our proposed method has relatively higher PSNR, lower spatial and temporal error than state-of-art algorithms. Future research directions include the robustness of the algorithm towards the errors introduced by motion estimation algorithms, and methods to restore texture areas.

VI. Acknowledgement

We would like to acknowledge the support of the Croucher Foundation scholarship, as well as the support of Samsung Information Systems America Inc. (SISA).

References

[1] Shin-Tson Wu and Deng-Ke Yang, *Fundamentals of Liquid Crystal Devices*, Wiley, Sep 2006, ISBN-13: 978-047001542.

[2] Erik Reinhard, Erum Arif Khan, Ahmet Oguz Akyuz, and Garrett Johnson, *Color Imaging Fundamentals and Applications*, A K Peters, 2008.

[3] N. Fisekovic, T. Nauta, H. Cornelissen, and J. Bruinink, "Improved motion-picture quality of AM-LCDs using scanning backlight,," *Proc. IDW*, pp. 1637–1640, 2001.

[4] Michael Becker, "LCD response time evaluation in the presence of backlight modulations," *SID Symposium Digest of Technical Papers*, vol. 39, no. 1, pp. 24–27, 2008.

[5] Koichi Oka and Yoshi Enami, "Moving picture response time (MPRT) measurement system," *SID Symposium Digest of Technical Papers*, vol. 35, pp. 1266–1269, 2004.

[6] Jae-Kyeong Yoon, Ki-Duk Kim, Nam-Yong Kong, Hong-Chul Kim, Tae-Ho You, Soon-Shin Jung, Gil-Won Han, Moojong Lim, Hyun-Ho Shin, and In-Jae Chung, "LCD TV comparable to CRT TV in moving image quality - worlds best MPRT LCD TV," in *Proc. of SPIE-IS&T Electronic Imaging*, 2007, vol. 6493.

[7] Hung-Xin Zhao, Mu-Lin Chao, and Feng-Chou Ni, "Overdrive LUT optimization for LCD by box motion blur measurement and gamma-based thresholding method," *SID Symposium Digest of Technical Papers*, vol. 39, no. 1, pp. 117–120, 2008.

[8] Haiying Wang, Thomas X Wu, Xinyu Zhu, and Shin-Tson Wu, "Correlations between liquid crystal director reorientation and optical response time of a homeotropic cell," *Journal of Applied Physics*, vol. 95, no. 10, pp. 5502–5508, 2004.

[9] Sunkwang Hong, Brian Berkeley, and Sang Soo Kim, "Motion image enhancement of LCDs," in *Proc. International Conference on Image Processing*. IEEE, 2005.

[10] BW. Lee, K. Song, DJ. Park, Y. Yang, U. Min, S. Hong, C. Park, M. Hong, and K. Chung, "Mastering the moving image: Refreshing TFT-LCDs at 120 hz," in *SID Symposium Digest of Technical Papers*. SID, 2005.

[11] N. Mishima and G. Itoh, "Novel frame interpolation method for hold-type displays," in *Proc. International Conference on Image Processing*, 2004, vol. 3, pp. 1473–1476.

[12] Yen Lin Lee and Truong Nguyen, "Fast one-pass motion compensated frame interpolation in high-definition video processing," in *Proceedings of IEEE International Conference on Image Processing*, November 2009, pp. 369–372.

[13] Suk-Ju Kang, Kyoung-Rok Cho, and Young Hwan Kim, "Motion compensated frame rate up-conversion using extended bilateral motion estimation," *IEEE Transactions on Consumer Electronics*, vol. 53, no. 4, pp. 1759–1767, Nov 2007.

[14] Hanfeng Chen, Sung-Soo Kim, Sung-Hee Lee, Oh-Jae Kwon, and Jun-Ho Sung, "Nonlinearity compensated smooth frame insertion for motion-blur reduction in lcd," in *IEEE 7th Workshop on Multimedia Signal Processing*. IEEE, Nov 2005, pp. 1–4.

[15] M. Klompenhouwer and L. Velthoven, "Motion blur reduction for liquid crystal displays: Motion compensated inverse filtering," in *Proceedings of SPIE-IS&T Electronic Imaging*. SPIE, 2004.

[16] F. H. Heesch and M.A. Klompenhouwer, "Spatio-temporal frequency analysis of motion blur reduction on LCDs," in *in International Conference on Image Processing*, 2007, vol. 4, pp. 401–404.

[17] Shay Har-Noy and Truong Q. Nguyen, "LCD motion blur reduction: A signal processing approach," *IEEE Transaction on Image Processing*, vol. 17, pp. 117–125, Feb 2008.

[18] Yonatan Wexler, Eli Shechtman, and Eli Shechtman, "Space-time completion of video," *IEEE Transcations on Pattern recongition and Machine Intelligence*, vol. 29, pp. 1–14, March 2007.

[19] Hao Pan, Xiao-Fan Feng, and Scott Daly, "LCD motion blur modeling and analysis," in *Proc. International Conference on Image Processing*. IEEE, 2005.

[20] Haiyan He, Velthoven L.J., E. Bellers, and J.G. Janssen, "Analysis and implementation of motion compensated inverse filtering for reducing motion blur on LCD panel," in *Digest of Technical Papers. International Conference on Consumer Electronics, 2007. ICCE 2007*, 2007, pp. 6.3–1.

[21] T. Kurita, "Moving picture quality improvement for hold-type AM-LCDs," *SID Symposium Digest of Technical Papers*, p. 986989, 2001.

[22] Sylvain Tourancheau, Kjell Brunnstrm, Brje Andrn, and Patrick Le Callet, "LCD motion-blur estimation using different measurement methods," *Journal of the Society for Information Display*, vol. 17, no. 3, pp. 239–249, March 2009.

[23] Michiel A. Klompenhouwer, "Temporal impulse response and bandwidth of displays in relation to motion blur," *SID Symposium Digest of Technical Papers*, vol. 36, pp. 1578–1581, May 2005.

[24] Michiel A. Klompenhouwer, "Comparison of LCD motion blur reduction methods using temporal impulse response and MPRT," *SID Symposium Digest of Technical Papers*, vol. 37, pp. 1700–1703, 2006.

[25] S. Yao, G. Feng, X. Lin, K.P. Lim, and W. Lin, "A coding artifacts removal algorithm based on spatial and temporal regularization," in *IEEE International Conference on Image Processing*, 2003, vol. 2, pp. 215–218.

[26] Yao Wang, Jorn Ostermann, and Ya-Qin Zhang, *Video Processing and Communications*, Prentice Hall, 2002.

[27] Yoon Kim, Kang-Sun Choi, Jae-Young Pyun, Byung-Tae Choi, and Sung-Jea Ko, "A novel de-interlacing technique using bi-directional motion estimation," in *Computational Science and Its Applications*, Heidelberg, 2003, vol. 2667 of *Lecture Notes in Computer Science*, p. 971, Springer Berlin.

[28] Stanley Chan, Dung Vo, and Truong Nguyen, "Subpixel motion estimation without interpolation," in *IEEE International Conference on Acoustics, Speech and Signal Processing*, 2010, pp. 722–725.

[29] Xiaofan Feng, Hao Pan, and Scott Daly, "Comparison of motion blur measurement in LCD," *SID Symposium Digest of Technical Papers*, vol. 38, no. 1, pp. 1126–1129, May 2007.

[30] Keith Rayner, "Eye movements in reading and information processing: 20 years of research," *Psychological Bulletin*, vol. 124, no. 3, pp. 372–422, 1998.

[31] E. Matin, "Saccadic suppression: A review," *Psychological Bulletin*, vol. 81, pp. 899–917, 1974.

[32] W. R. Uttal and E. Smith, "Recognition of alphabetic characters during voluntary eye movements," *Perception & Psychophysic*, vol. 3, pp. 257–264, 1968.

[33] Joyce Westerink and Kees Teunissen, "Perceived sharpness in complex moving images," *Display*, vol. 16, no. 2, pp. 89–97, 1995.

[34] David Burr, "Motion smear," *Nature*, vol. 284, no. 13, pp. 164–165, 1980.

[35] Thomas Bonse, "Visually adapted temporal subsampling of motion information," *Signal Processing: Image Communication*, vol. 6, pp. 253–266, 1994.

[36] J.W. Miller and E. Ludvigh, "The effect of relative motion on visual acuity," *Survey of Ophthalmology*, vol. 7, pp. 83–116, 1962.

[37] W. Glenn and K. Glenn, "Discrimination of sharpness in a televised moving image," *Displays*, vol. 6, pp. 202–206, 1985.

[38] Karl R. Gegenfurtner, Dajun Xing, Vrian Scott, and Michael Hawken, "A comparison of pursuit eye movement and perceptual performance in speed discrimination," *Journal of Vision*, vol. 3, pp. 865–876, 2003.

[39] Stanley Chan and Truong Nguyen, "Fast LCD motion deblurring by decimation and optimization," in *International Conference on Acoustics, Speech and Signal Processing*, 2009, pp. 1201–1204.

[40] Christopher C. Paige and Michael A. Saunders, "LSQR: An algorithm for sparse linear equations and sparse least squares," *ACM Transactions on Mathematmal Software*, vol. Vol 8, no. 1, pp. 43–71, March 1982.

[41] Report 1082-1, "Studies toward the unification of picture assessment methodology," Tech. Rep., ITU, 1986.

[42] Rafael C. Gonzalez and Richard E. Woods, *Digital Image Processing*, Prentice Hall, 2007.

[43] Sina Farsiu, Dirk Robinson, Michael Elad, and Peyman Milanfar, "Fast and robust multi-frame super-resolution," *IEEE Transactions on Image Processing*, vol. 13, pp. 1327–1344, 2004.

[44] Sina Farsiu, Dirk Robinson, Michael Elad, and Peyman Milanfar, "Advances and challenges in super-resolution," *International Journal of Imaging Systems and Technology, Special Issue on High Resolution Image Reconstruction*, vol. 14, no. 2, pp. 47–57, 2004.

[45] Sina Farsiu, Michael Elad, and Peyman Milanfar, "Video-to-video dynamic super-resolution for grayscale and color sequences," *EURASIP J. Appl. Signal Process.*, pp. 232–232, 2006.

[46] L. Rudin, S. Osher, and E. Fatemi, "Nonlinear total variation based noise removal algorithms," *Physics D*, vol. 60, pp. 259–268, Nov 1992.

[47] Michael K. Ng, Huanfeng Shen, Edmund Y. Lam, and Liangpei Zhang, "A total variation regularization based super-resolution reconstruction algorithm for digital video," *EURASIP Journal on Advances in Signal Processing*, p. 74585, 2007.

[48] Jose M. Bioucas-Dias, Mario A. T. Figueiredo, and Joao P. Oliveira, "Total variation-based image deconvolution: a majorization-minimization approach," in *Proceedings of IEEE Internation Conference on Acoustics, Speech and Signal Processing (ICASSP)*, May 2006, vol. 2, pp. 861–864.

[49] Byunggyoo Kim, *Numerical Optimization Methods for Image Restoration*, Ph.D. thesis, Stanford University, Dec 2002.

[50] Michael K. Ng, *Iterative Methods for Toeplitz Systems*, Oxford University Press, Inc, 2004.

[51] Yumei Huang, Michael Ng, and Youwei Wen, "A fast total variation minimization method for image restoration," *SIAM Multiscale model and simulation*, vol. 7, pp. 774–795, 2008.

[52] Yilun Wang, Junfeng Yang, Wotao Yin, and Yin Zhang, "An efficient TVL1 algorithm for deblurring multichannel images corrupted by impulsive noise," Tech. Rep., CAAM, Rice University, Sep 2008.

[53] D. Geman and G. Reynolds, "Constrained restoration and the recovery of discontinuities," *IEEE Transactions on Pattern Analysis and Machine Intelligence*, vol. 14, pp. 367–383, 1992.

[54] D. Geman and C. Yang, "Nonlinear image recovery with half-quadratic regularization," *IIEEE Transactions on Image Processing*, vol. 4, pp. 932–946, 1995.

[55] Y. Nesterov, "Smooth minimization of non-smooth functions," *Mathematical Programming*, vol. 103, pp. 127–152, 2005.

[56] Antonin Chambolle, "An algorithm for total variation minimization and applications," *Journal of Mathematical Imaging and Vision*, vol. 20, no. 1-2, pp. 89–97, 2004.

[57] Stephen Boyd, Lin Xiao, and Almir Mutapcic, "Subgradient methods," Classnote of EE 392O, Stanford University, Oct 2003, avaiable at http://www.stanford.edu/class/ee392o/subgrad_method.pdf.

[58] Dimitri Bertsekas, *Constrained Optimization and Lagrange Multiplier Methods*, Academic Press, 1982.

[59] N. Z. Shor, *Minimization Methods for Non-differentiable Functions*, Springer Series in Computational Mathematics. Springer, 1985.

[60] Philip Gill, Walter Murray, and Margaret Wright, *Practical Optimization*, Academic Press, 1981.

[61] J. Nocedal and S. Wright, *Numerical Optimization*, Springer, second edition, 2000.

[62] N. Nguyen, P. Milanfar, and G. H. Golub, "A computationally efficient image superresolution algorithm," *IEEE Trans. Image Processing*, vol. 10, pp. 573–583, Apr 2001.

[63] Per Christian Hansen, *Rank-deficient and discrete ill-posed problems*, SIAM, 1998.

[64] Xiang Zhu and Peyman Milanfar, "A no-reference sharpness metric sensitive to blur and noise," in *1st International Workshop on Quality*

of Multimedia Experience (QoMEX), July 2009, available at http://users.soe.ucsc.edu/~milanfar/publications/conf/qomex_zhu.pdf.

[65] Report BT.500-11, "Methodology for the subjective assessment of the quality of television pictures," Tech. Rep., ITU, 2002.

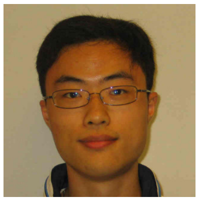

Stanley H. Chan [S'06] is currently a PhD student at the ECE Dept., University of California, San Diego. He received M.A. in applied mathematics from UCSD in June 2009, and B.Eng with first class honor in electrical engineering from the University of Hong Kong in June 2007. His research interests are large-scale numerical optimization algorithms with applications to video processing. Mr. Chan is a recipient of Croucher Foundation Scholarship.

Truong Q. Nguyen [F'05] is currently a Professor at the ECE Dept., UCSD. His research interests are video processing algorithms and their efficient implementation. He is the coauthor (with Prof. Gilbert Strang) of a popular textbook, Wavelets and Filter Banks, Wellesley-Cambridge Press, 1997, and the author of several matlab-based toolboxes on image compression, electrocardiogram compression and filter bank design. He has over 300 publications.

Prof. Nguyen received the IEEE Transaction in Signal Processing Paper Award (Image and Multidimensional Processing area) for the paper he co-wrote with Prof. P. P. Vaidyanathan on linear-phase perfect-reconstruction filter banks (1992). He received the NSF Career Award in 1995 and is currently the Series Editor (Digital Signal Processing) for Academic Press. He served as Associate Editor for the IEEE Transaction on Signal Processing 1994-96, for the Signal Processing Letters 2001-2003, for the IEEE Transaction on Circuits and Systems from 1996-97, 2001-2004, and for the IEEE Transaction on Image Processing from 2004-2005.